Channel-Optimized Quantum Error Correction

Soraya Taghavi
Department of Electrical Engineering and the Center for Quantum Information Science and Technology, University of Southern California, Los Angeles, CA 90089

Robert L. Kosut
SC Solutions, Systems & Control Division, 1261 Oakmead Pkwy., Sunnyvale, CA 94085

Daniel A. Lidar
Departments of Electrical Engineering, Chemistry, and Physics, and the Center for Quantum Information Science and Technology, University of Southern California, Los Angeles, CA 90089

arXiv:0810.2524v1 [quant-ph] 14 Oct 2008

We develop a theory for finding quantum error correction (QEC) procedures which are optimized for given noise channels. Our theory accounts for uncertainties in the noise channel, against which our QEC procedures are robust. We demonstrate via numerical examples that our optimized QEC procedures always achieve a higher channel fidelity than the standard error correction method, which is agnostic about the specifics of the channel. This demonstrates the importance of channel characterization before QEC procedures are applied. Our main novel finding is that in the setting of a known noise channel the recovery ancillas are redundant for optimized quantum error correction. We show this using a general rank minimization heuristic and supporting numerical calculations. Therefore, one can further improve the fidelity by utilizing all the available ancillas in the encoding block.

PACS numbers:

I. INTRODUCTION

Quantum error correction is often considered the backbone of quantum information processing, since it converts what is essentially an analog information processor, subject to a continuum of errors, into a digital one, whose errors are discretized. The theory of quantum error correction was developed in analogy to classical coding for noisy channels [1–6]. These initial efforts focused on finding conditions and procedures for perfect recovery of quantum states passing through noisy channels. Recently, several authors considered error correction design as an optimization problem, with fidelity as the optimization target [7–10]. In this work we further develop the theory of optimal quantum error correction. As in [7–10], we consider the scenario where one has knowledge of the noise channel, and find correspondingly optimal codes. That is, we assume that one has already performed a channel identification procedure, e.g., via quantum process tomography [11]. We show how, armed with a knowledge of the channel, one can design highly robust error correction procedures, whose fidelity is always at least as good as that of the "agnostic" codes of standard error correction [1–6].

More specifically, we present an indirect approach to fidelity maximization based on minimizing the error between the actual channel and the desired channel. This approach, like the previously developed approach to direct fidelity optimization, leads naturally to bi-convex optimization problems, namely, two semidefinite programs (SDPs) [12] which can be iterated between the recovery and encoding. For a given encoding the problem is convex in the recovery. For a given recovery, the problem is convex in the encoding. An important advantage of this approach is that noisy channels, which do not satisfy the standard assumptions for perfect correction [1–6], can be optimized for the best possible encoding and recovery.

The conventional fidelity optimization targets are the encoding and recovery operators. An important way in which the present work differs from previous studies is in the fact that we further add the distribution of the ancillas in the encoding and recovery to the optimization problem. This way, we utilize all possible degrees of freedom for optimization. As a consequence, we find a rather surprising result: in the optimized error correction procedure the fidelity is indifferent to the existence of the recovery ancillas. This result paves the way toward a more efficient utilization of the ancillas. Namely, we can use all the available ancilla qubits in the encoding to increase the fidelity.

Standard error correction schemes, as well as those produced by the aforementioned optimization methods which are tuned to specific errors, are often not robust to even small changes in the error channel. These errors can be mitigated by fault-tolerant methods which rely on several levels of code concatenation [13]. However, our method naturally enjoys a desirable robustness against error variations. We show a means to incorporate specific models of error channel uncertainty, resulting in highly robust error correction. Nevertheless, concatenated fault tolerant quantum error correction still enjoys a certain important advantage over the procedures we derive in this work, namely, it is robust also against imperfections in the encoding and recovery procedures, while here, as is the case for standard quantum error correction formulations, we assume these to be perfectly executed.

Since the number of optimization variables scales exponentially with the number of qubits used in the encoding and recovery operations, the computational effort required to solve any of the semidefinite program optimization (SDP) problems

is similarly burdened. In order to reduce this effort we propose an approach based on optimization via the constrained least squares method. This alternative approach for solving the indirect optimization problem does not utilize semidefinite programming, and is significantly faster in our numerical simulations. Surprisingly, this method returns the exact same result as the SDP approach.

The organization of the paper is as follows. In Section II, we explain the problem formulation including the standard error correction model and state the direct and indirect optimization problems to be addressed. The indirect approach is explored in Section III. In Section IV, we investigate the optimal distribution of the ancillas between the recovery and encoding. Examples of the methods presented are given in Section V. Appendices A-E provide proofs and supporting material.

II. PROBLEM FORMULATION

A. Standard error correction model

Subject to the assumption that the initial system-bath state is classically correlated [14], the dynamics of an open quantum system can be represented in an elegant form known as the Kraus *operator sum representation* (OSR). In this representation, the noise $\mathcal{E}$ is described in terms of a completely-positive (CP) map: $\rho \to \sum_i A_i \rho A_i^\dagger$ [6]. Here ρ is the initial system density matrix and the operators A_i, known as Kraus operators, or operation elements, satisfy the normalization relation $\sum_i A_i^\dagger A_i = I$ (identity). The standard error correction procedure involves CP encoding ($\mathcal{C}$), error ($\mathcal{E}$), and recovery ($\mathcal{R}$) maps (or channels): $\rho_{\rm S} \stackrel{\mathcal{C}}{\to} \rho_{\rm C} \stackrel{\mathcal{E}}{\to} \sigma_{\rm C} \stackrel{\mathcal{R}}{\to} \hat{\rho}_{\rm S}$, as shown pictorially in the block diagram of Figure 1.

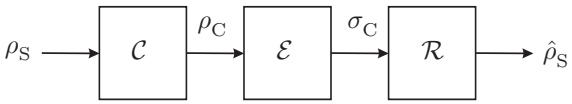

FIG. 1: Standard representation of error correction.

Here $\rho_{\rm S}$ is the $n_S \times n_S$ system state, $\rho_{\rm C}$ is the $n_C \times n_C$ encoded state, $\sigma_{\rm C}$ is the $n_C \times n_C$ perturbed encoded state, and $\hat{\rho}_{\rm S}$ is the $n_S \times n_S$ recovered system state. Using the OSR:

$$\hat{\rho}_{\rm S} = \sum_{r,e,c} (R_r E_e C_c) \rho_{\rm S} (R_r E_e C_c)^\dagger. \tag{1}$$

The encoding $\{C_c\}_{c=1}^{m_C}$ and recovery $\{R_r\}_{r=1}^{m_R}$ operation elements are rectangular matrices, respectively $n_C \times n_S$ and $n_S \times n_C$, since they map between the system Hilbert space of dimension n_S and the system/ancillas Hilbert space, the *codespace*, of dimension n_C. The error operation elements $\{E_e\}_{e=1}^{m_E}$ are square $(n_C \times n_C)$ matrices, and represent the effects of noise on the codespace. The number of elements, m_C, m_E, m_R depend on the manner of implementation and basis representation [6]. More specifically, any OSR can be equivalently expressed, and consequently physically implemented, as a unitary with ancilla states [6, §8.23]. An example of this representation of the standard error correction model of Figure 1 is shown in the block diagram of Figure 2.

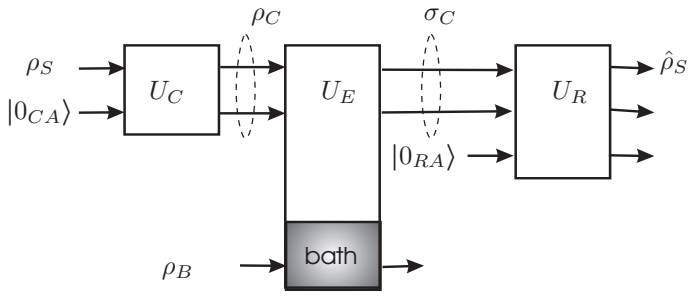

FIG. 2: System-ancilla-bath representation of standard encoding-error-recovery model of error correction.

In this case the encoding operation $\mathcal{C}$ is implemented by a unitary operator U_C acting on the (tensor) product of the system state, $\rho_{\rm S}$, and the encoding ancillas' state, $|0_{CA}\rangle$, producing the encoded state $\rho_{\rm C} = U_C(|0_{CA}\rangle\langle 0_{CA}| \otimes \rho_{\rm S})U_C^\dagger$. (The tensor ordering is arbitrary, but once established must remain fixed for consistency). If the encoding ancillas' state has dimension n_{CA}, then the resulting codespace has dimension $n_C = n_S n_{CA}$. If, as is customary, we take $|0_{CA}\rangle$ as the n_{CA}-column vector with a one in the first element and zeros elsewhere (*i.e.*, it is a tensor product of $\log_2 n_{CA}$ encoding ancillas, each in the state $|0\rangle = (1,0)^t$), then the OSR for $\mathcal{C}$ has the *single* ($m_C = 1$) $n_C \times n_S$ matrix element C whose columns are the first n_S columns of U_C, thus forming a set of orthonormal *codewords*, *i.e.*,

$$U_C = [C \ \cdots], \ C \text{ is } n_C \times n_S \tag{2}$$

For the errors, $\mathcal{E}$, the ancillas' states are not implemented by design, but rather, engendered by interaction with the *bath*, a term used to generically describe the physical environment. The error operation is thus equivalent to the unitary U_E operating on the tensor product of $\rho_{\rm C}$, the encoded state, and ρ_B, the bath state. The number of bath states may be very large, in principal infinite dimensional. However, it is always possible to represent $\mathcal{E}$ with a finite number of OSR elements with $m_E \le {n_C}^2$ [6, Thm.8.3].

Finally, the recovery operation $\mathcal{R}$ can be implemented via the unitary U_R operating on the (tensor) product of the perturbed encoded state, $\sigma_{\rm C}$, and the (additional) recovery ancillas' state $|0_{RA}\rangle$. If $|0_{RA}\rangle$ is an n_{RA}-column vector with a one in the first element and zeros elsewhere, then the OSR $\{R_r\}_{r=1}^{m_R}$ for $\mathcal{R}$ has $m_R = n_{CA} n_{RA}$ elements which consist of the first n_C columns of U_R, *i.e.*,

$$U_R = [R \ \cdots], \ R = \begin{bmatrix} R_1 \\ \vdots \\ R_{m_R} \end{bmatrix}, \ R_r \text{ is } n_S \times n_C \tag{3}$$

The model represented in Figures 1 and 2 assumes that the encoding and recovery operations can be implemented much

TABLE I: Definitions of some frequently used symbols.

Symbol	Definition
n_S	dimension of the system space
n_{CA}	dimension of the encoding ancillas space
n_C	dimension of the (system + encoding ancillas) space, *i.e.*, $n_C = n_S \times n_{CA}$
n_{RA}	dimension of the recovery ancillas space
m_E	number of operation elements for error map
m_R	number of operation elements for recovery map

faster than relevant time-scales associated with the bath. For a detailed discussion of the validity of such a Markovian model see [18]. Nevertheless, we will assume the model of Figures 1 and 2 for the remainder of this work, as complications associated with the bath being "on" during encoding and recovery are likely to be dealt with via fault tolerance methods [19], which require a base level of encoding of the type we find here.

Table I provides definitions of some frequently used symbols.

B. Performance measures

Assume that we are given the OSR elements of the error channel $\mathcal{E}$. This could be obtained, for example, from the output of a quantum process tomography experiment [11]. The error correction objective considered here is to design the encoding $\mathcal{C}$ and the recovery $\mathcal{R}$ so that, for a given error operation $\mathcal{E}$, the map $\rho_S \rightarrow \hat{\rho}_S$ is as close as possible to a desired $n_S \times n_S$ unitary logic gate L_S. Common measures of performance between two quantum channels are typically based on *fidelity* or *distance* [6], [20], [21], [22]. Here we will use the *channel fidelity* [7] between the error correction operation $\mathcal{REC}$ and the desired operation L_S:

$$f = \frac{1}{n_s^2} \sum_{r,e,c} |\mathbf{Tr}\ L_S^\dagger R_r E_e C_c|^2. \tag{4}$$

where $0 \leq f \leq 1$ and from [5], [6, Thm.8.2], $f = 1$ if and only if there are constants δ_{rec} such that,

$$R_r E_e C_c = \delta_{rec} L_S,\ \sum_{r,e,c} |\delta_{rec}|^2 = 1. \tag{5}$$

This suggests the *indirect* measure of fidelity, the "distance-like" error (using the Frobenius norm, $\|X\|_{\mathrm{F}}^2 = \mathbf{Tr}\ X^\dagger X$),

$$\begin{array}{rcl} d &=& \sum_{r,e,c} \|R_r E_e C_c - \delta_{rec} L_S\|_{\mathrm{F}}^2 \\ &=& \sum_c \|RE(I_E \otimes C_c) - \Delta_c \otimes L_S\|_{\mathrm{F}}^2 \end{array} \tag{6}$$

where

$$\Delta_c \equiv [\delta_{rec}], \quad \dim \Delta_c = m_R \times m_E, \tag{7}$$

and E is the $n_C \times n_C m_E$ rectangular "error matrix,"

$$E = [E_1\ \cdots\ E_{m_E}], \tag{8}$$

R is the $m_R n_S \times n_C$ matrix obtained by stacking the m_R matrices R_r as in (3), and I_E is the $m_E \times m_E$ identity. Hence, we have $\sum_c \mathbf{Tr}\ \Delta_c^\dagger \Delta_c = \sum_{r,e,c} |\delta_{rec}|^2 = 1$, and $R^\dagger R = \sum_r R_r^\dagger R_r = I_C$.

We show in Appendix A that there exists a recovery and encoding pair, $\mathcal{R}, \mathcal{C}$, which achieves perfect error correction (equivalently $d = 0,\ f = 1$), iff for $c, c' = 1, \ldots, m_C$

$$(I_E \otimes C_c^\dagger) E^\dagger E (I_E \otimes C_{c'}) = \Delta_c^\dagger \Delta_{c'} \otimes I_S \tag{9}$$

This is a generalization to non-unitary CP encoding of the Knill-Laflamme condition for perfect error correction with unitary encoding [5]. In this latter case, $\mathcal{C}$ has only a single $n_C \times n_S$ matrix element $C,\ C^\dagger C = I_S$, whose n_S columns are the *codewords*. As f and d are explicitly dependent on the channel elements, they are convenient for optimization. Consider then the following optimization problems.

Direct Fidelity Maximization

$$\begin{array}{ll} \text{maximize} & f(R, C) \\ \text{subject to} & R^\dagger R = I_C,\ \ C^\dagger C = I_S \end{array} \tag{10}$$

Indirect Fidelity Maximization

$$\begin{array}{ll} \text{minimize} & d(R, C, \Delta_1, \ldots, \Delta_{m_C}) \\ \text{subject to} & R^\dagger R = I_C,\ \ C^\dagger C = I_S,\ \ \sum_c \|\Delta_c\|_{\mathrm{F}}^2 = 1 \end{array} \tag{11}$$

Here C is the $n_C \times n_S$ matrix obtained in (2) . The direct approach was used in [7, 9, 10, 15–17]. As shown in Appendix B, f and d are related as follows:

$$\begin{array}{rcl} f(R, C) &=& \left(1 - \hat{d}(R, C)/2n_S\right)^2 \\ \hat{d}(R, C) &=& \min\left\{ d(R, C, \Delta_1, \ldots, \Delta_{m_C}) \,\middle|\, \|\Delta_c\|_{\mathrm{F}}^2 = 1,\ \forall c \right\} \end{array} \tag{12}$$

This shows that minimizing the distance (11) is equivalent to

maximizing fidelity (10).

C. Robust error correction

An important advantage of the method presented here is that unlike the standard error correction model, it accounts for uncertainty in knowledge of the channel. Such uncertainty may exist for many reasons. For example, different runs of a tomography experiment can yield different error channels $\{\mathcal{E}_\alpha\}_{\alpha=1}^{\ell}$. Or, a physical model of the error channel might be generated by a Hamiltonian $H(\theta)$ dependent upon an uncertain set of parameters θ. In any case, not accounting for the uncertainties typically leads to non-robust error correction, in the sense that a small change in the error model can lead to poor performance of the error correction procedure. One way to account for these Hamiltonian parametric uncertainties is to take a sample from the set of Hamiltonians, say, $\{H(\theta_\alpha)\}_{\alpha=1}^{\ell}$. Tracing out the m_E bath states will result in a *set* of error channels $\{\mathcal{E}_\alpha\}_{\alpha=1}^{\ell}$ where each error channel has OSR elements $\{E_{\alpha,k}\}_{k=1}^{\kappa}$, where κ is the largest of the number of OSR elements in each sample. In those samples with a smaller number we can set the corresponding OSR elements to zero.

Two standard measures of robustness are the *average-case* and *worst-case*. For the average-case, suppose that each OSR set $\mathcal{E}_\alpha$ is known to occur with probability p_α. Then define the *average error channel* by the OSR,

$$\mathcal{E}^{\rm avg} = \{\ \sqrt{p_\alpha}E_{\alpha,k}\ |\, \alpha = 1,\ldots,\ell, k = 1,\ldots,\kappa\ \} \qquad (13)$$

The average error channel in this form has $\kappa\ell$ OSR elements, potentialy a very large number. However, this number is readily reduced to no more than $m_E = n_C^2$ using a singular value decompostion [6, Thm.8.3]. Associated with $\mathcal{E}^{\rm avg}$ is the average channel fidelity,

$$f^{\rm avg} = \sum_\alpha p_\alpha f_\alpha = \frac{1}{n_S^2}\sum_{r,e',c} |\mathbf{Tr}\ R_r E_{e'}^{\rm avg} C_c|^2 \qquad (14)$$

where $E_{e'}^{\rm avg},\ e' = 1,\ldots,\ell\kappa$ are the OSR elements of $\mathcal{E}^{\rm avg}$ in (13).

For average-case robust error correction we replace f in (10) with $f^{\rm avg}$ in (14), and using the relationship (12), replace d in (11) with,

$$\begin{array}{rcl} d^{\rm avg} &=& \|RE^{\rm avg}(I_E\otimes C) - \Delta\otimes L_S\|_{\rm F}^2 \\ E^{\rm avg} &=& [E_1^{\rm avg}\ \cdots\ E_{\ell\kappa}^{\rm avg}] \end{array} \qquad (15)$$

A similar formulation exists for worst-case error correction which was considered in [10]; we do not consider it any further here. The remainder of the paper concentrates on the average-case objective and development of the associated optimization algorithms. The examples presented in Sec.V show that this approach yields a high degree of robustness to uncertainty in the optimal codes.

We now discuss methods to approximately solve (obtain local solutions to) the indirect optimization problem (11).

III. INDIRECT FIDELITY MAXIMIZATION

We consider the encoding operator $\mathcal{C}$ as a unitary operator acting on both the encoding ancillas and the input qubit. Using the constraints in (11), we can express the distance measure (6) as

$$\begin{aligned} d(R,C,\Delta) &= \|RE(I_E\otimes C) - \Delta\otimes L_S\|_{\rm F}^2 \qquad (16)\\ &= n_S + \mathrm{Tr}\ E(I_E\otimes CC^\dagger)E^\dagger - 2\mathrm{Re\ Tr} RE(\Delta^\dagger\otimes CL_s^\dagger) \end{aligned}$$

where Δ is the *single* $m_R\times m_E$ matrix in (7) with $m_R = n_{CA}n_{RA}$ (note that in this case, since there is only a single Δ_c matrix, we drop the subscript c).

A. Optimal Recovery

Since only the last term in (16) depends on the recovery matrix R, minimizing $d(R,C,\Delta)$ with respect to R is equivalent to maximizing the last term. In Appendix A, we show that this maximization results in

$$\max_{R^\dagger R = I_C} \mathrm{Re\ Tr}\ RE(\Delta^\dagger\otimes CL_s^\dagger) = \mathrm{Tr}\sqrt{E(\Gamma\otimes CC^\dagger)E^\dagger}, \qquad (17)$$

where the $m_E\times m_E$ matrix Γ is defined as,

$$\Gamma = \Delta^\dagger\Delta, \qquad (18)$$

and the associated $n_Cn_{RA}\times n_C$ optimal recovery matrix is,

$$R = [v_1\ ...\ v_{n_C}][u_1\ ...\ u_{n_C}]^\dagger \qquad (19)$$

where $v_i,\ u_i,\ i = 1,\ldots,n_C$ are, respectively, the right and left singular vectors in the singular value decomposition of the $n_C\times n_Cn_{RA}$ matrix $E(\Delta^\dagger\otimes CL_S^\dagger)$, with the singular values, as usual, in descending order. Thus, to obtain the optimal recovery, we need first to find Γ which maximizes (17) – this is equivalent to minimizing d over R. Following this we need to determine Δ satisfying (18).

To find Γ, observe that $\Gamma\ge 0$ by definition (18), and the constraint $\|\Delta\|_{\rm F} = 1$ from (11) is equivalent to $\mathrm{Tr}\ \Gamma = 1$. Hence, optimal recovery can be obtained by first solving for Γ from,

$$\begin{array}{ll} \text{maximize} & \mathrm{Tr}\sqrt{E(\Gamma\otimes CC^\dagger)E^\dagger} \\ \text{subject to} & \Gamma\ge 0,\ \mathrm{Tr}\,\Gamma = 1 \end{array} \qquad (20)$$

In Appendix D it is shown that the optimal Γ is the solution of an equivalent SDP.

The next step is to use (18) to obtain Δ from Γ. The fol-

lowing choice adheres to the given dimensions:

$$\begin{pmatrix} n_{CA} \le m_E \\ n_{RA} n_{CA} = m_E \end{pmatrix} \Rightarrow \begin{cases} \Delta = \sqrt{\Gamma} \\ R \text{ is tall } (n_S m_E \times n_C) \end{cases}$$
$$\begin{pmatrix} n_{CA} > m_E \\ n_{RA} = 1 \end{pmatrix} \Rightarrow \begin{cases} \Delta = \begin{bmatrix} \sqrt{\Gamma} \\ 0_{n_{CA}-m_E \times m_E} \end{bmatrix} \\ R \text{ is unitary } (n_C \times n_C) \end{cases} \tag{21}$$

Clearly the choice of Δ is not unique. In fact, the result does not change if Δ is multiplied by a unitary, *i.e.*, $\Delta \to U\Delta$. This is exactly the unitary freedom in choosing the OSR elements [6]. Interestingly, however, from many numerical calculations we observe that the following holds:

$$\begin{cases} \text{rank}(\Gamma) = n_{CA} \text{ if } n_{CA} \le m_E \\ \text{rank}(\Gamma) = m_E \text{ if } n_{CA} > m_E. \end{cases} \tag{22}$$

Since the $m_E \times m_E$ matrix Γ is Hermitian ($= \Delta^\dagger \Delta$), and Δ is $m_R \times m_E$ with $m_R = n_{CA} n_{RA}$, it follows that if (22) is true then,

$$n_{RA} = 1. \tag{23}$$

If, in the optimized error correction, *the dimension of the recovery ancillas space is one, then the optimal recovery matrix R is always a unitary – recovery ancillas are redundant in maximizing the fidelity.* Note that we started with a generic n_{RA} parameter, and the properties of the optimal solution led us to the above conclusion. Although we do not have a rigorous proof that the recovery ancillas are redundant, a compelling heuristic argument is offered in Section IV along with supporting numerical results.

B. Optimal Encoding

For a given R and Δ, the optimal encoding C can be found by solving (11) for C, that is,

$$\begin{aligned} &\text{minimize} \quad d(R, C, \Delta) = \|RE(I_E \otimes C) - \Delta \otimes L_S\|_{\text{F}}^2 \\ &\text{subject to} \quad C^\dagger C = I_S \end{aligned} \tag{24}$$

As shown in Appendix E, the optimal encoding C is given by,

$$C = UV^\dagger \tag{25}$$

where (U, V) are obtained from the SVD,

$$\bar{C} = \sum_{r,e} \delta_{re} (R_r E_e)^\dagger L_S = USV^\dagger$$

with U an $n_C \times n_S$ matrix with orthonormal columns, *i.e.*, $U^\dagger U = I_S$, V an $n_S \times n_S$ unitary, and S a diagonal matrix of the n_S singular values. The matrix $\bar{C}$ is the *unconstrained* (least-squares) solution to (24), *i.e.*, $\min_C d$.

The left-hand column of Table II, labeled Algorithm-1, summarizes the preceding method for recovery and encoding optimization. For optimal recovery alone, solve (20) for Γ, then determine Δ via (21), and finally R from (19). For optimal encoding alone, solve (24) for C. To find a combined optimal encoding and recovery repeat steps 1 and 2 in Table II until d stops decreasing. (By virtue of (12), fidelity increases in every step). Since in each step the distance measure, d, can only decrease, never increase, the converged solution to the combined optimization is only guaranteed to be a local optimal solution to (11).

C. Alternative iterative algorithm for recovery optimization

An alternative to the above optimal recovery procedure (Step 1 in Algorithm-1of Table II) is to iterate between solving (11) *directly* by minimizing over Δ and then using (19) to find R. Specifically, for a given R and C, Step 2a in Algorithm-2of Table II requires solving the following constrained least-squares problem for Δ:

$$\begin{aligned} &\text{minimize} \quad d(R, C, \Delta) = \|RE(I_E \otimes C) - \Delta \otimes L_S\|_{\text{F}}^2 \\ &\text{subject to} \quad \|\Delta\|_{\text{F}} = 1 \end{aligned} \tag{26}$$

As shown in Appendix B, the solution is,

$$\begin{aligned} \Delta &= \bar{\Delta}/\|\bar{\Delta}\|_{\text{F}} \\ \left(\bar{\Delta}\right)_{re} &= \mathbf{Tr}(R_r E_e C L_S^\dagger)/n_S, \end{aligned} \tag{27}$$

where $\bar{\Delta}$ is the unconstrained (least squares) solution to $\min_\Delta d$. This solution is then used in (19) to find R (Step 1b), then back to (27) (Step 1a), and so on until d stops decreasing (Step 1c).

The difference between the two algorithms is in computing the optimal recovery (Steps 1). In Step 1 of Algorithm-1, no iterations are required; the optimal recovery is achieved by solving the SDP (20). For Step 1 of Algorithm-2, an optimal recovery is the result of some number of iterations involving the constrained least-squares problem (26). Although at present a proof is not available, in every case we have tried the optimal fidelity in both recovery algorithms converges to the same result. Additionaly, the total CPU-time in MATLAB to compute the optimal recovery in Algorithm-2 (including the iterations) is significantly less than the CPU-time for the recovery step in Algorithm-1 using YALMIP [28] to call the solver SDPT3 [29].

TABLE II: Iterative Algorithms for Optimal QEC

Algorithm-1	**Algorithm-2**
Initialize R and C	**Initialize** R and C
Repeat	**Repeat**
1. **Optimal recovery**	1. **Optimal recovery** – Repeat a-c
(a) solve (20) for Γ	(a) solve (26) for Δ
(b) $\Gamma \rightarrow \Delta$ via (21)	(b) $\Delta \rightarrow R$ via (19)
(c) $\Delta \rightarrow R$ via (19)	(c) Until d stops decreasing
2. **Optimal encoding**	2. **Optimal encoding**
(a) solve (24) for C	(a) solve (24) for C
Until d stops deceasing	**Until** d stops deceasing

IV. DIMENSION OF THE RECOVERY ANCILLAS SPACE

In our formalism, the dimension of the Recovery ancillas' space, *i.e.*, the required number of recovery ancilla qubits, is determined by the rank of the $m_E \times m_E$ matrix Γ.

A. Rank minimization of Γ

In this section, we study the rank of Γ through a heuristic argument by noting the similarity between our problem and the so called "Rank Minimization Problem" (RMP) [24]:

$$\begin{array}{ll} \text{minimize} & \text{rank}\,(X) \\ \text{subject to} & X \in \mathcal{X} \end{array} \tag{28}$$

The matrix X is the optimization variable and $\mathcal{X}$ is a convex set denoting the constraints.

Although several special cases of the RMP have well-known solutions, in general the RMP is known to be computationally intractable. However, there are a number of heuristic approaches to solving this problem. Restate (20) as follows,

$$\begin{array}{ll} \text{minimize} & \text{Tr}\,(\Gamma) \\ \text{subject to} & \Gamma \geq 0,\ \ \text{Tr}\sqrt{E(\Gamma \otimes CC^\dagger)E^\dagger} \geq \text{const.} \end{array} \tag{29}$$

where the constant is the maximum which arose in (20). A well known heuristic for RMP when X is positive semidefinite [25–27] is to replace the rank objective with Tr $[X]$ and solve,

$$\begin{array}{ll} \text{minimize} & \text{Tr}\,[X] \\ \text{subject to} & X \in \mathcal{X},\ X \geq 0 \end{array} \tag{30}$$

By comparing (29) with (30), we can view our problem in (20) as an RMP that minimizes the rank of Γ. Thus, the rank of the optimal Γ is the smallest possible consistent with not changing the rank of our objective matrix, $\sqrt{E(\Gamma \otimes CC^\dagger)E^\dagger}$. Noting that rank$(CC^\dagger) = n_S$ and rank$(E) = n_C$ and with a straightforward linear algebra analysis we find that this property holds if

$$\begin{cases} \text{rank}(\Gamma) \geq n_{CA} \ \text{ if } \ n_{CA} \leq m_E \\ \text{rank}(\Gamma) = m_E \ \text{ if } \ n_{CA} > m_E. \end{cases} \tag{31}$$

That is, in the first case, if rank$(\Gamma) < n_{CA}$, rank$(\sqrt{E(\Gamma \otimes CC^\dagger)E^\dagger})$ decreases by decreasing the rank of Γ. But if rank$(\Gamma) \geq n_{CA}$, rank$(\sqrt{E(\Gamma \otimes CC^\dagger)E^\dagger}) = n_C$, and it does not depend on rank(Γ). In the second case, Γ should be full rank. Therefore the rank of the optimal Γ is

$$\begin{cases} \text{rank}(\Gamma_{\text{opt}}) = n_{CA} \ \text{ if } \ n_{CA} \leq m_E \\ \text{rank}(\Gamma_{\text{opt}}) = m_E \ \text{ if } \ n_{CA} > m_E, \end{cases} \tag{32}$$

which agrees with (22). Note that the same argument also applies in the average case (15) with E replaced by E^{avg}.

B. Numerical result for randomly generated error maps

Here, we examine the result above for randomly generated error maps. Namely, we find the rank of the optimal Γ for each random map by applying the indirect optimization method. The error map is modeled as shown in Fig. 2 as a unitary U_E acting on the joint codespace-bath Hilbert space. The unitary U_E arises from a randomly selected $m_E n_C \times m_E n_C$ time-independent Hamiltonian H_E, *i.e.*, $U_E = e^{-itH_E}$ (we work in units where $\hbar = 1$). The unitary evolution operator generated

by this Hamiltonian at time $t = 1$ is

$$U_E = \exp(-iH_E) = \begin{bmatrix} E_1 & \dots \\ E_2 & \dots \\ \vdots & \\ E_{m_E} & \dots \end{bmatrix} \tag{33}$$

That is, we pick the first n_C columns of the matrix U_E. Here, $E_1 \dots E_m$ are the $n_C \times n_C$ OSR elements of the error operation, and from (8), $E = [E_1 \ \cdots \ E_{m_E}]$.

Figure 3 presents the channel fidelity *vs.* the number of iterations in Algorithm 1 for 100 random error maps. In this experiment, the system is a single qubit and one qubit is used as an encoding ancilla, *i.e.*, $n_S = 2$, $n_{CA} = 2$. Each error map has 4 OSR elements, *i.e.*, $m_E = 4$, and is generated using a 16×16 random Hamiltonian matrix according to (33). Therefore, the matrix Γ in (20) is 4×4. Figure 4 shows the histogram of the rank of Γ *vs.* the number of iterations. This histogram indicates that after 20 iterations in the optimization algorithm, the rank of Γ is always two, which is equal to n_{CA}. In fact, those Γ that are not rank 2 after 10 iterations are associated to the error maps with lower rate of fidelity convergence.

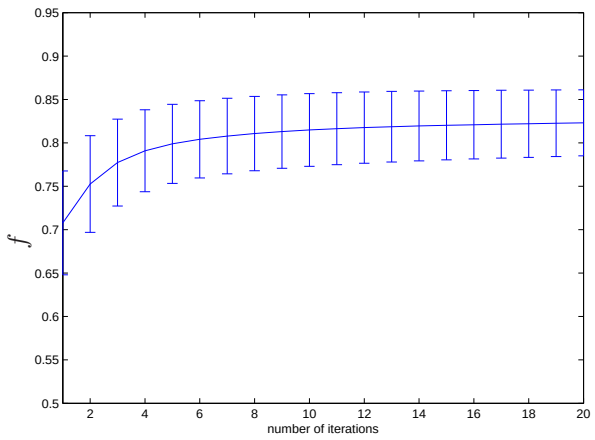

FIG. 3: Channel fidelity f for random error maps on two-qubit codes.

Figure 5, which shows the singular values of the same Γ matrices, is included for comparison of the magnitude of the singular values. In all cases, the nonzero singular values are of the order of 10^{-1}. The numerical precision of all the results is 10^{-8}. We repeated the experiment for more than 1000 random maps with different dimensions (only 100 are shown), and the result holds for all of them. Namely, after sufficiently many iterations in Algorithm 1, *the rank of the optimal* Γ *is the same as the dimension of the encoding ancillas space, i.e., rank* $(\Gamma_{opt}) = n_{CA}$.

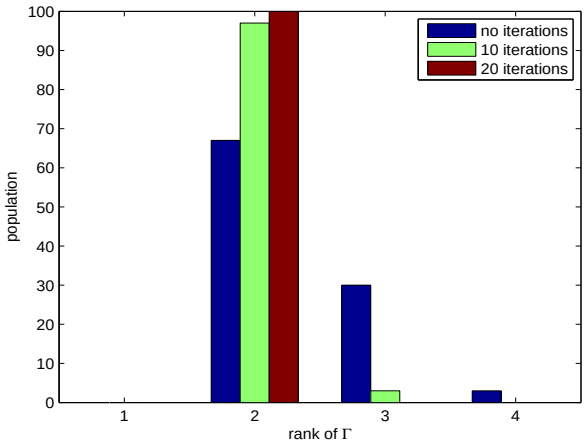

FIG. 4: Rank of the optimal Γ for random error maps on two-qubit codes.

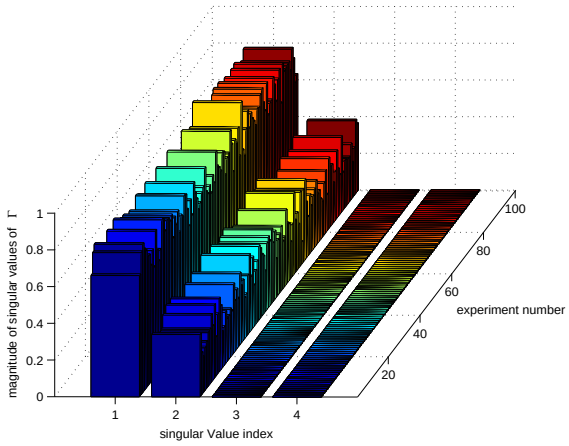

FIG. 5: Singular values of the optimal Γ for random error maps on two-qubit codes. For all cases tested only two of the singular values are significantly different from zero, meaning that the rank of the Γ matrices is 2.

V. EXAMPLES

We now apply the methods developed above to the goal of preserving a single qubit ($n_S = 2$) using a q_C-qubit ($n_C = 2^{q_C}$) codespace. In these examples, the error channel $\mathcal{E}$ consists of single-qubit errors occurring *independently* on all qubits with probability p. We examine two cases of bit-flip and bit-phase-flip errors.

A. 3-qubit bit-flip errors

In this example, we consider the independently occurring bit-flip error as the noise channel, where the bit-flip operator

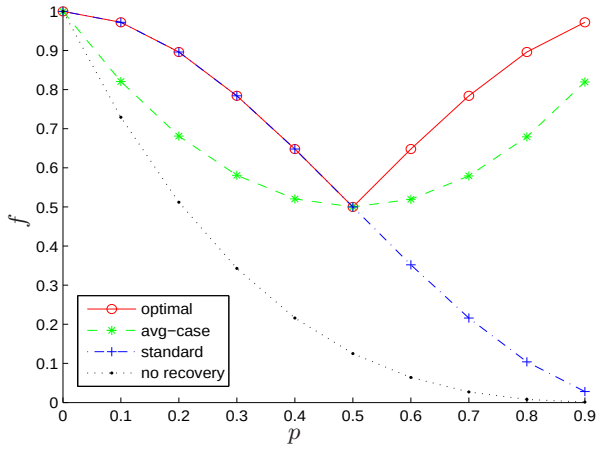

FIG. 6: Channel fidelity f *vs.* bit-flip probability p for 3-qubit encoding.

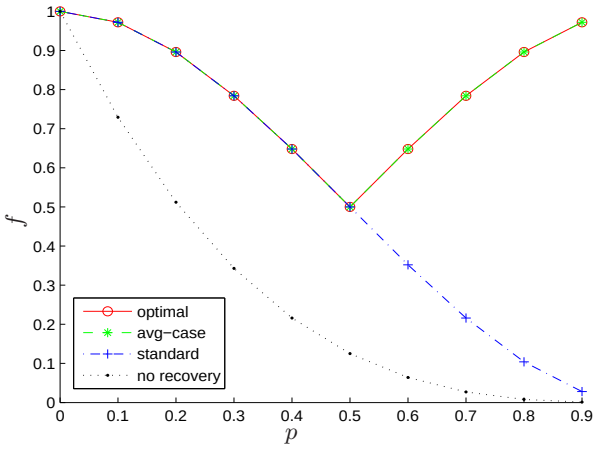

FIG. 7: Channel fidelity f *vs.* bit-flip probability p for 3-qubit encoding in two ranges: $p < 0.5$ and $0.5 < p \leq 0.9$.

is $X = \begin{bmatrix} 0 & 1 \\ 1 & 0 \end{bmatrix}$. We used $q_C = 2$ encoding ancilla qubits. There are $2^3 = 8$ OSR error elements for 3-qubit encoding:

$$\begin{aligned} \{E_i\}_{i=1}^{8} &= A_{i_1} \otimes A_{i_2} \otimes A_{i_3}, \quad i_1, i_2, i_3 \in \{1, 2\} \\ A_1 &= \sqrt{(1-p)}\, I \quad (\text{no error}) \\ A_2 &= \sqrt{p}\, X \quad (\text{bit} - \text{flip error}) \end{aligned} \tag{34}$$

Figure 6 shows f *vs.* bit-flip probability p in the range $p \leq 0.9$ for the standard 3-qubit code, optimal recovery at each p, average-case recovery over the p range, and no recovery. For the average case, we computed an optimized encoding and recovery for the single channel obtained by averaging over the error channels corresponding to $p = 0, 0.1, ..., 0.9$ as defined in (15). We then applied this encoding and recovery to each of these 10 channels, thus producing the 10 fidelity values shown. Note that the optimal recovery can be achieved equivalently by either the constrained least squares method (Algorithm-2) or the convex optimization method (Algorithm-1). Interestingly, the standard 3-qubit code not only provides optimal recovery for the range $p \leq 0.5$, it is optimal for *both* recovery and encoding in this range. For $p > 0.5$ the standard code is clearly no longer optimal. Only in this range does the optimal recovery outperform the standard code, a phenomenon similar to what was reported for amplitude-damping errors in [7]. Analysis of our optimal encoding recovery results reveals the following simple picture. The optimal code is the standard 3-qubit code for the entire p range, *i.e.*, $|\bar{0}\rangle = |000\rangle$ and $|\bar{1}\rangle = |111\rangle$. The optimal recovery is the standard recovery [6] in the range $0 \leq p \leq 0.5$. In the range $0.5 \leq p \leq 0.8$ the optimal recovery is a bit-flip on all qubits followed by the standard recovery.

Figure 7 shows channel fidelity f in two ranges: $p < 0.5$ and $0.5 < p \leq 0.9$. Unlike the previous case, here we compute the optimization twice, once for each range. For the average case, we computed an optimized encoding and recovery for the single channel obtained by averaging over the error channels corresponding to $p = 0, 0.1, ..., 0.4$. We then applied this encoding and recovery to each of these 5 channels, thus producing the 5 fidelity values shown in the range $0 \leq p \leq 0.5$. We then repeated this procedure for $p = 0.5, 0.6, ..., 0.9$. For $p < 0.5$, the standard, optimal, average-case, all coincide. For $p > 0.5$, the optimal and average-case codes coincide and divert again from the standard. The optimal encoding and recovery are the same as in Figure 6, *i.e.*, the standard 3-qubit code, with standard recovery in the range $0 \leq p \leq 0.5$, and bit-flips preceeding standard recovery in the range $0.5 \leq p \leq 0.9$. We conclude from the examples in Figures 6 and 7 that optimal encoding and recovery has no advantage over standard encoding and recovery for low bit-flip probabilities ($p < 0.5$), and thus increasing the codespace would be required to improve fidelity. For large errors ($p > 0.5$), optimization is more effective in that it identifies an optimal recovery. In both cases the achieved optimal fidelity is independent of the number of recovery ancillas used, hence in all examples shown in Figures 6 and 7 there are no additional recovery ancillas required. It is striking that the average case fidelity matches the optimal in Figure 7, but not in Figure 6. This is entirely due to the range of p values over which the average is performed. The lesson is that the more information is available about the noise channel, the more robust the encoding and recovery will be: in Figure 7 we know that the probability is in the range $[0, 0.5]$ or $[0.5, 0.9]$, while in Figure 6 we only know that it is in the range $[0, 0.9]$. Absent such information, robustness may still be attainable by experimenting with tuning the encoding and recovery over a range of channels.

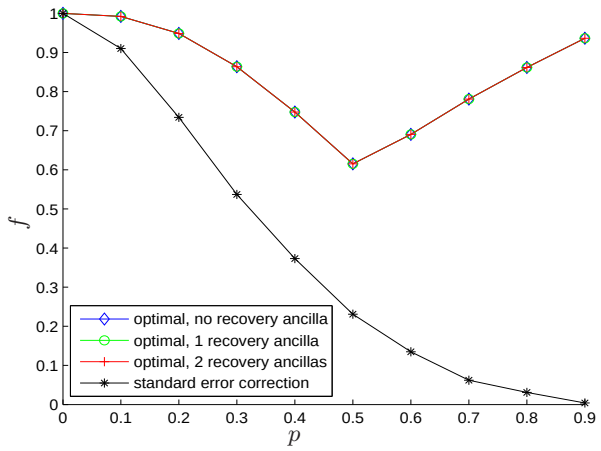

FIG. 8: Channel fidelity f *vs.* bit-phase flip probability p for 3 qubit code and 0, 1, or 2 recovery ancillas, with optimal encoding and recovery.

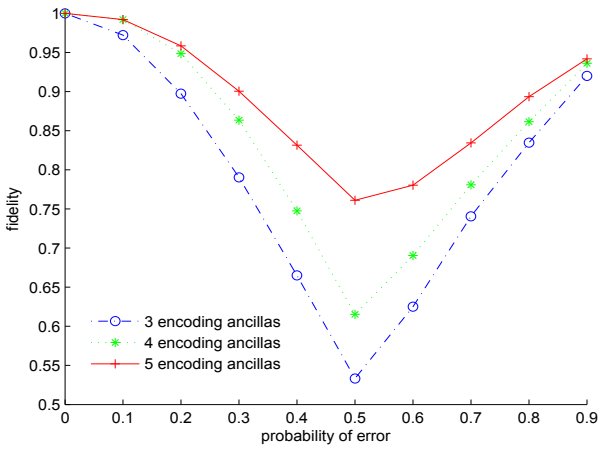

FIG. 9: Channel fidelity f *vs.* bit-phase flip probability p with a fixed total of 6 ancillas, and optimal encoding and recovery.

B. Bit-Phase flip error

In this example, the noise channel consists of bit-phase flip errors $Y = \begin{bmatrix} 0 & -i \\ i & 0 \end{bmatrix}$ occurring independently with probability p. We do not allow for more than three to occur simultaneously (*i.e.*, we consider weight-3 errors). We examine two cases: 1. Considering a fixed number of encoding ancillas, we compare the fidelity using different numbers of recovery ancillas. 2. We fix the total number of available ancilla qubits, and compare the fidelity for various distributions of encoding and recovery ancillas.

1. 5-qubit bit-phase flip error

In this example, the bit-phase flip errors occur independently on the input qubit and 4 ancillas. There are 26 error OSR elements: 1 for no error, 5 for a single error, 10 for double errors, and 10 for triple errors. Thus the matrix Γ in (20) is 26×26 and the rank of $\Gamma_{\rm opt}$ is equal to $n_{CA} = 16$, meaning that the optimal distribution of ancillas is having all four in the encoding block and none in the recovery block.

Figure 8 shows f *vs.* bit-phase flip error probability p for the optimal encoding/recovery in the case of zero, one and two recovery ancillas. The result shows that all cases yield the same fidelity. Therefore, the fidelity of the system is independent of the number of recovery ancillas.

2. bit-phase flip errors with a fixed number of ancillas

In this example, we consider six ancilla qubits that can be used either in the encoding block or in the recovery block. We compare the fidelity for the following distributions: four encoding ancillas and two recovery ancillas, five encoding ancillas and one recovery ancilla, and six encoding ancillas with no recovery ancilla. Figure 9 shows that the channel fidelity increases significantly by using the ancillas in the encoding instead of the recovery. Thus the most efficient use of ancillas is achieved when they are all used for encoding.

VI. CONCLUSION

We have presented an optimization approach to quantum error correction that yields codes which achieve robust performance, when tuned to a specific noise channel. An important aspect of developing optimal codes which are tuned to a class of errors, or are robust over a range of errors, is that the optimized performance levels may be sufficient for the intended purposes. *Hence, no further increases in codespace dimension may be necessary.* This cannot be known without performing the optimization.

We also showed that the fidelity of such a system is independent of the number of the recovery ancillas. This is entirely due to the structure of the error correction optimization problem, for which we found that a unitary recovery operator maximizes the fidelity of the system. However, the fidelity increases significantly by increasing the dimension of the encoding ancillas space. Therefore, in the optimal quantum error correction scheme, one should use all the available ancilla qubits in the encoding block.

Although not further developed here, the resulting codes, unlike standard codes, have support over all basis states. Some of the recovery structure is revealed via the indirect approach. This in turn leads to a method for approximating optimal recovery involving only a singular value decomposition, making it potentially useful in evaluating very large blocks of encoding to see if further performance improvement is possible.

We stress that there is an important difference between the standard error correction schemes [1–6] and the approach pre-

sented here. While in the standard case only the class of errors should be known, in our method the exact form of the noise map is required for optimization. In general, the noise map can be identified using quantum process tomography [11]. In most cases this extra knowledge is equivalent to identifying the probability of the error, which can also be found using our method. In order to identify the probability in a particular error model, one should calibrate the fidelity of the system using a fixed pair of recovery and encoding operators. Once the relation between the fidelity associated to this pair and the error probability is known, a measurement of the fidelity yields the probability.

It thus appears that the effectiveness of optimization is dependent upon the *structure* of the error operation, a result seemingly heralded by Feynman [30]:

> "In a machine such as this there are very many other problems due to imperfections. ... there may be small terms in the Hamiltonian besides the ones we've written. ... At least some of these problems can be remedied in the usual way by techniques such as error correcting codes ... But until we find a specific implementation for this computer, I do not know how to proceed to analyze these effects. However, it appears that they would be very important in practice. This computer seems to be very delicate and these imperfections may produce considerable havoc."

Determining the "specific implementation" is currently an on-going research effort. Analyzing the "effects" however will undoubtedly be accomplished by a combination of physical modeling and/or system identification (*e.g.,* process tomography and parameter estimation). This leads to an intriguing prospect: to integrate the results found here within a complete "black-box" error correction scheme, that takes quantum state or process tomography as input and iterates until it finds an optimal error correcting encoding and recovery.

Acknowledgments

Funded under the DARPA QuIST Program and (to D.A.L.) NSF CCF-0726439 and NSF PHY-0802678.

[1] P. W. Shor, Phys. Rev. A **52**, R2493 (1995).
[2] D. Gottesman, Phys. Rev. A **54**, 1862 (1996).
[3] A. M. Steane, Phys. Rev. Lett. **77**, 793 (1996).
[4] R. Laflamme, C. Miquel, J.P. Paz and W.H. Zurek, Phys. Rev. Lett. **77**, 198 (1996).
[5] E. Knill and R. Laflamme, Phys. Rev. A **55**, 900 (1997).
[6] M.A. Nielsen and I.L. Chuang, *Quantum Computation and Quantum Information* (Cambridge University Press, Cambridge, UK, 2000).
[7] M. Reimpell and R. F. Werner, Phys. Rev. Lett. **94**, 080501 (2005).
[8] N. Yamamoto, S. Hara, and K. Tsumara, Phys. Rev. A **71**, 022322 (2005).
[9] R. L. Kosut and D. A. Lidar, eprint quant-ph/0606078.
[10] R.L. Kosut, A. Shabani, and D.A. Lidar, Phys. Rev. Lett. **100**, 020502 (2008).
[11] J. F. Poyatos, J. I. Cirac, and P. Zoller, Phys. Rev. Lett. **78**, 390 (1997); I. L. Chuang and M. A. Nielsen, J. Mod. Opt. **44**, 2455 (1997); G. M. D'Ariano and P. Lo Presti, Phys. Rev. Lett. **86**, 4195 (2001); R. L. Kosut, I. A. Walmsley, and H. Rabitz, eprint quant-ph/0411093 (2004); M. Mohseni and D.A. Lidar, Phys. Rev. Lett. **97**, 170501 (2006).
[12] S. Boyd and L. Vandenberghe, *Convex Optimization* (Cambridge University Press, Cambridge, UK, 2004).
[13] F. Gaitan, *Quantum Error Correction and Fault Tolerant Quantum Computing* (CRC Press, Boca Raton, 2008).
[14] A. Shabani and D.A. Lidar, eprint arXiv.org:0808.0175.
[15] A. S. Fletcher, P. W. Shor, and M. Z. Win, Phys. Rev. A **75**, 012338 (2007).
[16] A. S. Fletcher, Ph.D. Dissertation, eprint arXiv:0706.3400.
[17] M. Reimpell, R.F. Werner, and K. Audenaert, eprint quant-ph/0606059.
[18] R. Alicki, D.A. Lidar, and P. Zanardi, Phys. Rev. A **73**, 052311 (2006).
[19] P. Aliferis, D. Gottesman, and J. Preskill, Quantum Inf. Comput. **6**, 97 (2006).
[20] A. Gilchrist, N. K. Langford, and M. A. Nielsen, Phys. Rev. A **71**, 062310 (2005).
[21] D. Kretschmann and R. F. Werner, New J. of Phys. **6**, 26 (2004).
[22] R. L. Kosut, M. Grace, C. Brif, and H. Rabitz, eprint quant-ph/0606064.
[23] R. Horn and C. Johnson. *Topics in Matrix Analysis* (Cambridge University Press, Cambridge, 1991).
[24] L. Vandenberghe and S. Boyd, SIAM Review **38**, 49 (1996).
[25] M. Fazel, "Matrix rank minimization with applications", PhD thesis, Dept. of Electrical Engineering, Stanford University (2002).
[26] M. Fazel, H. Hindi, and S. Boyd, Proc. American Control Conference, Boston, Massachusetts (2004).
[27] M. Mesbahi and G. P. Papavassilopoulos, IEEE Trans. on Automatic Control **42**, 23943 (1997).
[28] J. Lofberg. Yalmip: A toolbox for modeling and optimization in MATLAB. In *Proceedings of the CACSD Conference*, Taipei, Taiwan, 2004.
[29] K. C. Toh, R. H. Tutuncu, and M. J. Todd. Sdpt3: Matlab software for semidefinite-quadratic-linear programming. 2004. http://www.math.nus.edu.sg/∼mattohkc/sdpt3.html.
[30] R.P. Feynman, Found. Phys. **16**, 507 (1986).

APPENDIX A: PROOF OF EQUATIONS (9), (17), (19)

The $n_C \times n_C n_{RA}$ matrix $W = E(\Delta^\dagger \otimes C)$ has a maximum rank of n_C. Hence a singular value decomposition is of the form $W = USV^\dagger,\ S = [S_0\ 0]$, with S_0 an $n_C \times n_C$ diagonal matrix containing the n_C singular values. If V is partitioned as $V = [V_1\ V_2]$ with V_1 being $n_{RA}n_C \times n_C$ then the objective function in (17) becomes,

$$\mathrm{Re}\ \mathbf{Tr}\ RW = \mathrm{Re}\ \mathbf{Tr}\ S_0 X,\ X = V_1^\dagger RU \qquad \text{(A1)}$$

Since $\|X\| \leq 1$, then $\mathrm{Re}\ \mathbf{Tr}\ S_0 X \leq \mathbf{Tr}\ S_0$. Equality occurs if and only if $X = I_C$, or equivalently, $R = V_1 U^\dagger$, which is precisely the result in (19). This also establishes that the optimal objective function is $\mathbf{Tr}\ S_0$ which, by definition, is equal to $\mathbf{Tr}\sqrt{WW^\dagger}$, thus

$$\max_{R^\dagger R = I_C} \mathrm{Re}\mathbf{Tr}\ RW = \mathbf{Tr}\sqrt{WW^\dagger} \tag{A2}$$

which establishes (17).

Condition (9) follows directly from (5) by multiplying both sides by their respective conjugate (with indices c and c') which also eliminates R because $R^\dagger R = I_C$. This immediately establishes that (9) is a *necessary condition* for (5). To prove *sufficiency*, first expand (6) to get,

$$\begin{aligned} d &= \textstyle\sum_c \mathbf{Tr}\ (I_E \otimes C_c^\dagger) E^\dagger E (I_E \otimes C_c) \\ &\quad + \mathbf{Tr}\ \Gamma_c \otimes I_S - 2\mathrm{Re}\mathbf{Tr}\ RE(\Delta_c^\dagger \otimes C_c L_S^\dagger) \\ \Gamma_c &= \Delta_c^\dagger \Delta_c \end{aligned} \tag{A3}$$

From (A2), we get,

$$\begin{aligned} \min_{R^\dagger R = I_C} d &= \textstyle\sum_c [\mathbf{Tr}\ (I_E \otimes C_c^\dagger) E^\dagger E (I_E \otimes C_c) \\ &\quad + \mathbf{Tr}\ \Gamma_c \otimes I_S] - 2\mathbf{Tr}\sqrt{WW^\dagger} \\ W &= \textstyle\sum_c\ E(\Delta_c^\dagger \otimes C_c L_S^\dagger) \end{aligned} \tag{A4}$$

Using (9) we get, $\mathbf{Tr}\sqrt{WW^\dagger} = \sum_c\ E(I_E \otimes C_c C_c^\dagger) E^\dagger$. This, together with repeated uses of (9) shows that $\min_{R^\dagger R = I_C} d = 0$. Since d is a norm, and is zero, then so is its argument, which by definition establishes (5) and thus shows sufficiency of (9).

APPENDIX B: RELATION BETWEEN FIDELITY f AND DISTANCE d

The problem is,

$$\begin{aligned} &\text{minimize} \quad d = \textstyle\sum_c \|RE(I_E \otimes C_c) - \Delta_c \otimes L_S\|_{\mathrm{F}}^2 \\ &\text{subject to} \quad \textstyle\sum_c \|\Delta_c\|_{\mathrm{F}}^2 = 1 \end{aligned} \tag{B1}$$

Form the Lagrangian,

$$L = d + \lambda(\sum_c \mathbf{Tr}\ \Delta_c^\dagger \Delta_c - 1) \tag{B2}$$

with λ the Lagrange multiplier. Then, $\nabla_{\delta_{rec}} L = 0$ when $(n_S + \lambda)\delta_{rec} = \mathbf{Tr}\ R_r E_e C_c L_S^\dagger$. To enforce the constraint $\sum_c \|\Delta_c\|_{\mathrm{F}}^2 = 1$ requires that $(n_S + \lambda)^2 = \sum_{r,e,c} |\mathbf{Tr}\ R_r E_e C_c L_S^\dagger|^2$. Hence,

$$\begin{aligned} \Delta_c &= \bar{\Delta}_c / \sqrt{\textstyle\sum_c \|\bar{\Delta}_c\|_{\mathrm{F}}^2} \\ \bar{\delta}_{rec} &= \mathbf{Tr}(R_r E_e C_c L_S^\dagger)/n_S \end{aligned} \tag{B3}$$

Observe that $\sum_c \|\bar{\Delta}_c\|_{\mathrm{F}}^2 = f$. This together with $\sum_r R_r^\dagger R_r = I_C$, $\sum_c C_c^\dagger C_c = I_S$ gives the optimal distance as given implicitly by (12). Note also that with no constraint, $\lambda = 0$, the $\bar{\Delta}_c$ are the optimal least-squares (unconstrained) solution.

APPENDIX C: UNITARY FREEDOM IN EQUATION (17)

In (17), $\Gamma = \Delta^\dagger \Delta$ remains unchanged if Δ is multiplied by a unitary. This unitary freedom is exactly the unitary freedom in describing the error map OSR. To see this, recall again from [6, Thm.8.2] that two error maps with OSR elements $E = [E_1 \ldots E_{m_E}]$ and $F = [F_1 \ldots F_{m_E}]$ are equivalent if and only if $E_i = \sum_j W_{ij} F_j$ where the $m_E \times m_E$ matrix W is unitary. Equivalently from (A3), $E = F(W \otimes I_C)$. Substituting this for E into the left hand side of (17) gives,

$$\mathrm{Re}\ \mathbf{Tr}\ RE(\Delta^\dagger \otimes C L_S^\dagger) = \mathrm{Re}\ \mathbf{Tr}\ RF((\Delta')^\dagger \otimes C L_S^\dagger) \tag{C1}$$

with $\Delta' = \Delta W^\dagger$. Hence, $\Delta'^\dagger \Delta' = W \Delta^\dagger \Delta W^\dagger = \Gamma$, which establishes the claim.

APPENDIX D: SOLVING EQUATION (20) VIA AN SDP

Problem (20) is of the form,

$$\begin{aligned} &\text{maximize} \quad \mathbf{Tr}\sqrt{F(\Gamma)} \\ &\text{subject to} \quad \Gamma \geq 0,\ \mathbf{Tr}\ \Gamma = 1 \end{aligned} \tag{D1}$$

where $F(\Gamma)$ is linear in Γ. Consider the relaxed problem,

$$\begin{aligned} &\text{maximize} \quad \mathbf{Tr}\ Y \\ &\text{subject to} \quad F(\Gamma) - Y^2 \geq 0,\ \Gamma \geq 0,\ \mathbf{Tr}\ \Gamma = 1 \end{aligned} \tag{D2}$$

This is an SDP in Γ and Y with Lagrangian,

$$\begin{aligned} L(\Gamma, Y, P, Z) &= -\mathbf{Tr}\ Y - \mathbf{Tr}\ P(F(\Gamma) - Y^2) \\ &\quad - \mathbf{Tr}\ Z\Gamma + \lambda(\mathbf{Tr}\ \Gamma - 1) \end{aligned} \tag{D3}$$

The dual function is,

$$\begin{aligned} g(P, \lambda, Z) &= \inf_{\Gamma, Y} L(\Gamma, Y, P, Z) \\ &= \begin{cases} \inf_Y \mathbf{Tr}(PY^2 - Y) - \lambda, & Z = \lambda I - A(P) \\ -\infty & \text{otherwise} \end{cases} \end{aligned} \tag{D4}$$

with $A(P) = \frac{\partial}{\partial \Gamma} \mathbf{Tr}\ PF(\Gamma)$, which is not dependent on Γ because $F(\Gamma)$ is linear in Γ. Performing the indicated $\inf_Y$ gives $Y = (1/2)P^{-1}$ and $g = -(\lambda + (1/4)\mathbf{Tr}\ P^{-1})$. The dual optimization associated with (D2) is to maximize g, or equivalently, minimize its negative, *i.e.*,

$$\begin{aligned} &\text{minimize} \quad \lambda + \tfrac{1}{4}\mathbf{Tr}\ P^{-1} \\ &\text{subject to} \quad P > 0,\ \lambda I - A(P) \geq 0 \end{aligned} \tag{D5}$$

This is an SDP in the dual variables P, λ. For this problem *strong duality* holds [12]. Consequently, at optimality of (D2) and (D5) the complementary slackness condition is $P_{\mathrm{opt}}(F(\Gamma_{\mathrm{opt}}) - Y_{\mathrm{opt}}^2) = 0$. Since $P_{\mathrm{opt}} > 0$, we have

$Y_{\rm opt} = \sqrt{F(\Gamma_{\rm opt})}$. This establishes that solving the SDP (D2) is equivalent to solving the original problem (D1).

APPENDIX E: SOLVING FOR C IN EQUATION (24)

The problem is,

$$\begin{array}{ll} \text{minimize} & d = \sum_c \|RE(I_E \otimes C) - \Delta \otimes L_S\|_{\rm F}^2 \\ \text{subject to} & C^\dagger C = I_S \end{array} \tag{E1}$$

Form the Lagrangian,

$$L = d + \mathbf{Tr}\ P(C^\dagger C - I_S) \tag{E2}$$

with P the Lagrange multiplier. Then, $\nabla_C L = 0$ when $C = \bar{C}(I_S + P)^{-1}$ with $\bar{C}$ as defined in (24). To enforce the constraint $C^\dagger C = I_S$ requires that $(I_S + P)^2 = \bar{C}^\dagger \bar{C}$. Hence, $C = \bar{C}(\bar{C}^\dagger \bar{C})^{-1/2}$. The actual computation of C is done using the SVD (25)-(26). Note that with no constraint, $P = 0$, and $\bar{C}$ is the optimal least-squares (unconstrained) solution.